



Molecular dynamics investigations of structural and functional changes in Bcl-2 induced by the novel antagonist BDA-366

Tao Li^{a,b,c,*}, Yinglu Cui^{a,*} and Bian Wu^a 

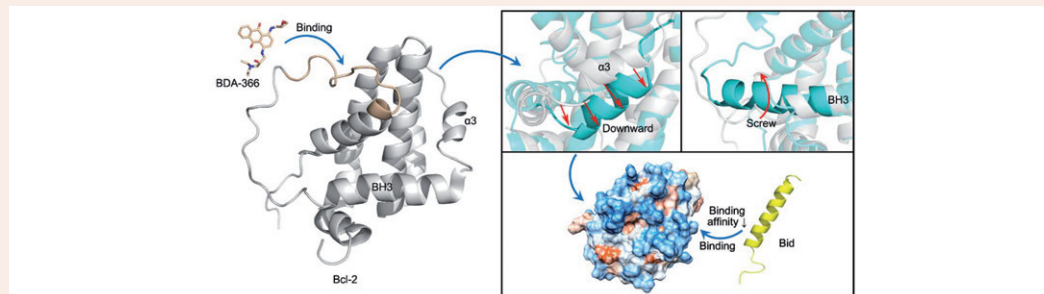
^aCAS Key Laboratory of Microbial Physiological and Metabolic Engineering, State Key Laboratory of Microbial Resources, Institute of Microbiology, Chinese Academy of Sciences, Beijing, P. R. China; ^bUniversity of Chinese Academy of Sciences, Beijing, P. R. China; ^cState Key Laboratory of Transducer Technology, Chinese Academy of Sciences, P. R. China

Communicated by Ramaswamy H. Sarma

ABSTRACT

Apoptosis is a fundamental biological phenomenon, in which anti- or proapoptotic proteins of the Bcl-2 family regulate a committed step. Overexpression of Bcl-2, the prototypical antiapoptotic protein in this family, is associated with therapy resistance in various human cancers. Accordingly, Bcl-2 inhibitors intended for cancer therapy have been developed, typically against the BH3 domain. Recent experimental evidences have shown that the antiapoptotic function of Bcl-2 is not immutable, and that BDA-366, a novel antagonist of the BH4 domain, converts Bcl-2 from a survival molecule to an inducer of cell death. In this study, the underlying mechanisms of this functional conversion were investigated by accelerated molecular dynamics simulation. Results revealed that Pro127 and Trp30 in the BH4 domain rotate to stabilize BDA-366 via π - π interactions, and trigger a series of significant conformational changes of the α 3 helix. This rearrangement blocks the hydrophobic binding site (HBS) in the BH3 domain and further prevents binding of BH3-only proteins, which consequently allows the BH3-only proteins to activate the proapoptotic proteins. Analysis of binding free energy confirmed that BDA-366 cross-inhibits BH3-only proteins, implying negative cooperative effects across separate binding sites. The newly identified blocked conformation of the HBS along with the open to closed transition pathway revealed by this study advances the understanding of the Bcl-2 transition from antiapoptotic to proapoptotic function, and yielded new structural insights for novel drug design against the BH4 domain.

GRAPHICAL ABSTRACT



The ability of the small molecule BDA-366 to convert Bcl-2 from an antiapoptotic to a proapoptotic molecule was investigated by accelerated molecular dynamics simulation. Results show that BDA-366 blocks or reduces the affinity of Bcl-2 for BH3-only proteins like Bid via negative cooperative effects, thereby releasing such proteins and unleashing their proapoptotic effects.

ARTICLE HISTORY

Received 6 February 2018
Accepted 22 May 2018

KEYWORDS

molecular dynamics; MM-GBSA; Bcl-2; conformational changes; accelerated molecular dynamics


Introduction

Apoptosis (programmed cell death) is an important biological process by which cells commit suicide after completing physiological function (Elmore, 2007; Kerr, Wyllie, & Currie, 1972). B cell leukemia/lymphoma 2 (Bcl-2) family proteins control a critical step in regulating apoptosis (Hardwick &

Soane, 2013). This family of interacting partners includes both proapoptotic and antiapoptotic members (Moldoveanu, Follis, Kriwacki, & Green, 2014). The balance between them is the major factor affecting the permeabilization of the mitochondrial outer membrane, which induces cytochrome c release and leads to activation of downstream caspases (Hardwick & Soane, 2013; Lopez & Tait, 2015). This pathway

CONTACT Bian Wu  wub@im.ac.cn

*Tao Li and Yinglu Cui contributed equally to this work.

 Supplementary data for this article can be accessed at [publisher website](https://www.tandfonline.com/doi/suppl/10.1080/07391102.2018.1491424).

© 2018 Informa UK Limited, trading as Taylor & Francis Group

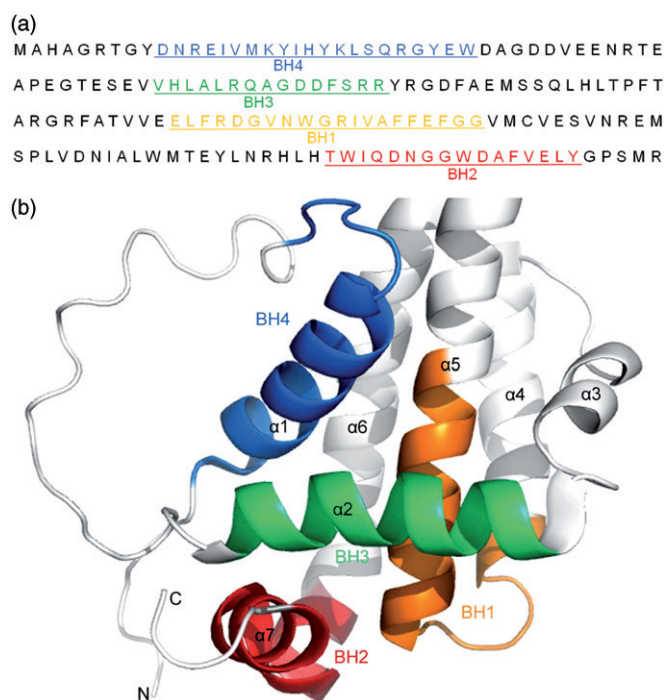


Figure 1. Homology domains (a) and three-dimensional structure (b) of antiapoptotic protein Bcl-2 (PDB: 1G5M) (Petros et al., 2001).

is required for normal embryonic development and for preventing cancer (Lopez & Tait, 2015; Ola, Nawaz, & Ahsan, 2011; Shamas-Din, Kale, Leber, & Andrews, 2013). The members of Bcl-2 family are usually classified into three distinct subclasses based on the presence of up to four conserved homology domains (BH) (Figure 1(a,b)) (Rajan, Choi, Baek, & Yoon, 2015). The apoptotic activating proteins (Bax, Bak, and Bok) which contain only BH1 to BH3 domains, belong to the proapoptotic subclass. These proteins induce apoptosis by triggering permeabilization of the mitochondrial outer membrane, then releasing apoptotic cytokines from mitochondria to cytosol (Antignani & Youle, 2006; Czabotar et al., 2013). The Bcl-2-like proteins (Bcl-2, Bcl-xL, Bcl-w, Mcl-1, A1, and Bcl-B), which contain all four BH1 to BH4 domains, constitute the antiapoptotic subclass. The proteins in this subclass inhibit apoptosis by sequestering BH3-only proteins to prevent oligomerization of Bax or Bak (Ku, Liang, Jung, & Oh, 2011). The third functional subgroup is designated BH3-only (Bid, Bim, Bad, Puma, and Noxa) subclass, which contains only the BH3 domain. The BH3 only members have high affinity for binding and activating Bax and Bak, but they can also be fettered by antiapoptotic proteins and thus lose the ability to activate Bax/Bak (Moldoveanu et al., 2013; Willis et al., 2007).

Bcl-2, the prototypical antiapoptotic protein in the family (Thomas et al., 2013), is strongly expressed in breast, prostate, colon, and non-small cell lung cancer and other tumours (Delbridge, Grabow, Strasser, & Vaux, 2016; Gibson & Davids, 2015; Lopez & Tait, 2015). Bcl-2 is composed of seven helices and one large flexible loop domain (Figure 1(b)) (Petros et al., 2001). Previous studies showed that antiapoptotic proteins were inhibited when their hydrophobic binding site (HBS), formed by the helices $\alpha 2$, $\alpha 3$, $\alpha 4$, and $\alpha 5$, were occupied by the BH3 helix of BH3-only family members (e.g.,

Bid) (Figure 2(a,c)) (Shamas-Din et al., 2013). Therefore, Bcl-2 inhibitors that mimic BH3-only proteins and mask the HBS have attracted tremendous attentions over the past decades as potential cancer therapeutics (Acoca, Cui, Shore, & Purisima, 2011; Delbridge et al., 2016; Thomas et al., 2013). Nevertheless, none of these inhibitors have been licensed for clinical use due to their limited efficacy or even off-target effects (Delbridge et al., 2016; Vela & Marzo, 2015).

The BH4 domain (Figure 2(b)), found exclusively in antiapoptotic subclass, represents a superior therapeutic target in light of its unique structure and crucial functions in suppressing apoptosis (Liu et al., 2016). Deletion of this domain completely eliminates the antiapoptotic activity of Bcl-2 without compromising the binding of BH3-only proteins (Han et al., 2015). In addition, Han et al. screened about 300,000 small molecules from the National Cancer Institute (NCI) and found compound NSC639366 also named as BDA-366 ($C_{24}H_{29}N_3O_4$, molecular weight [MW] 423.50, Figure 2(d)) had the most potent activity against human lung cancer cells (Han et al., 2015; Kolluri et al., 2008). This novel nonpeptide small-molecule antagonist of the BH4 domain was demonstrated to convert Bcl-2 from an antiapoptotic molecule to an inducer of cell death, and thus it is a promising anticancer drug candidate. However, experimental techniques such as immunoprecipitation and fluorescence polarization assays are insufficient to provide insights at atomic level into the allosteric functional conversion process.

Computational approaches such as molecular dynamics (MD) simulations could provide structural and functional details to answer biological and chemical questions with atomistic precision (Koshy, Parthiban, & Sowdhamini, 2010; Raghav, Verma, & Gangenahalli, 2012). However, large energy barriers during conformational transitions remain a grand challenge in conventional MD simulations. Accordingly, many simulation methods have been developed to investigate the allosteric effects induced by specific regulatory factors (Amadei, Linssen, & Berendsen, 1993; Do & Troisi, 2015; Hamelberg, Mongan, & McCammon, 2004; Miao, Feixas, Eun, & McCammon, 2015; Raghav et al., 2012). One drawback of these enhanced sampling techniques is the requirement of predefined reaction coordinates. In comparison, accelerated molecular dynamics (aMD) is widely used to improve sampling of the conformational space by reducing energy barriers in conformational transitions with no such requirement (Hamelberg et al., 2004; Markwick & McCammon, 2011; Miao et al., 2015). Kalenkiewicz, Grant, and Yang (2015) have combined aMD and conventional MD to enhance sampling of the conformations of the HBS in Bcl-xL, and thereby elucidated the interactions between the site and its ligands. Similarly, Schiott et al. (Andersen et al., 2017) gained insights from aMD simulations of the conformational transition of $\alpha 1$ AT from the biologically active metastable state to the loop-inserted thermodynamically relaxed.

Of note, the structural and dynamic behaviors of Bcl-2 apo form or Bcl-2-Bid complex with binding of BDA-366 are not easily accessible in conventional MD. Hence, aMD was used in this study to investigate the atomistic, allosteric, and functional consequences of BDA-366 binding to the BH4

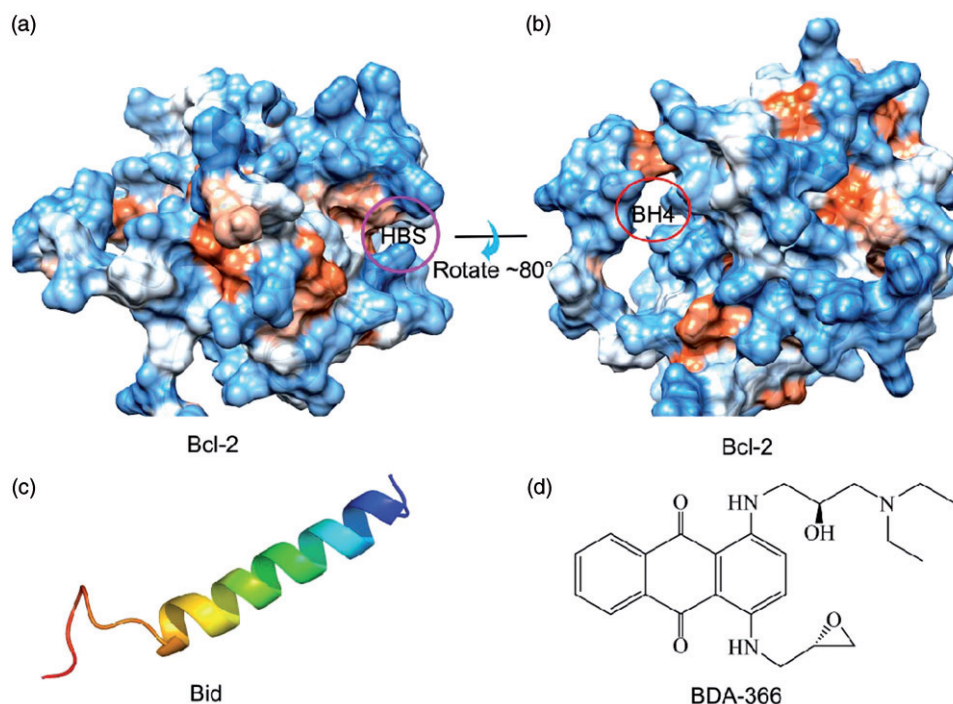


Figure 2. The HBS (a) and the BH4 domain (b) in Bcl-2, which interacts with Bid (c), and BDA-366 (d), respectively. (a and b) The protein surface was colored by wettability, blue represents hydrophilic and orange represents hydrophobic.

domain. A negative cooperative model was also proposed for the cross-inhibitory effects of BDA-366 across distinct binding sites in Bcl-2. Finally, the data provide a theoretical indication for the future development of drugs against the BH4 domain.

Materials and methods

Model preparation

To date, the structures of two isoforms of human Bcl-2 apo forms have been determined (PDB: 1G5M, 1GJH) (Petros et al., 2001), as well as those of human Bcl-2 with a bound ligand (PDB: 1YSW, 2O2F, and 2O21) (Bruncko et al., 2007; Ku et al., 2011; Oltersdorf et al., 2005; Perez et al., 2012). 1GJH was obtained from 1G5M by mutating residue 96 from an alanine to a threonine and residue 110 from a glycine to an arginine (Petros et al., 2001), while 1YSW (Oltersdorf et al., 2005), 2O2F and 2O21 (Bruncko et al., 2007) were in complex with BH3-mimetic inhibitors. Other structures such as 2XA0 (Ku et al., 2011), 4IEH (Toure et al., 2013), and 4AQ3 (Perez et al., 2012) lack the flexible loop domain. Therefore, 1G5M was selected as the initial Bcl-2 structure.

Molecular docking

BDA-366 was docked into the BH4 domain in 1G5M using Autodock 4.2 (Morris et al., 2009). The simulation box was fixed around BH4, with box size 80 Å in all three dimensions, and with all other parameters set to default values. Collected conformations were then clustered based on the root-mean-square deviations (RMSD) against the conformation with the lowest binding energy (Shao, Tanner, Thompson, & Cheatham, 2007). Finally, the complex with the highest score among the top 100

docked conformations was selected as the starting structure for subsequent MD simulation. BDA-366 was also docked into a representative conformation of the Bcl-2-Bid complex, which was obtained from the highest occurrence cluster of Bcl-2-Bid simulation using average-linkage clustering algorithm.

Protein docking

Crystal structures of Bid bound to Bcl-xL (PDB: 4QVE) and Mcl-1 (PDB: 5C3F) have been determined (Miles et al., 2016; Rajan et al., 2015). In the latter, the mutated Bid peptide exhibits incomplete sequences, and Mcl-1 has larger RMSD against 1G5M (2.57 Å) than Bcl-xL in 4QVE (1.035 Å). Thus, 4QVE was selected as the reference structure for the Bcl-2-Bid complex.

Z-dock (Pierce et al., 2014) was used to dock Bid into Bcl-2 structure. The receptor binding site residues were set to residues 101-120, 129-137, 143-151, and 197-203 based on the binding mode of 4QVE crystal structure. As before, collected conformations were clustered based on RMSD against 4QVE, and the complex with the lowest binding energy among the 100 top docked conformations was selected as the initial structure for MD simulation.

MD simulation

Bcl-2-BDA-366, Bcl-2-Bid, and Bcl-2-Bid-BDA-366 complexes were simulated in AMBER 16 (Case et al., 2016; Do & Troisi, 2015) using the ff14SB force field. The structural optimization of BDA-366 was conducted using B3LYP combined with 6-31 + G* basis set using the Gaussian09 software (Frisch et al., 2016). RESP fitting procedure was used for charge derivation based on the optimal conformation. Finally, the force field parameters of BDA-366 were derived using the antechamber

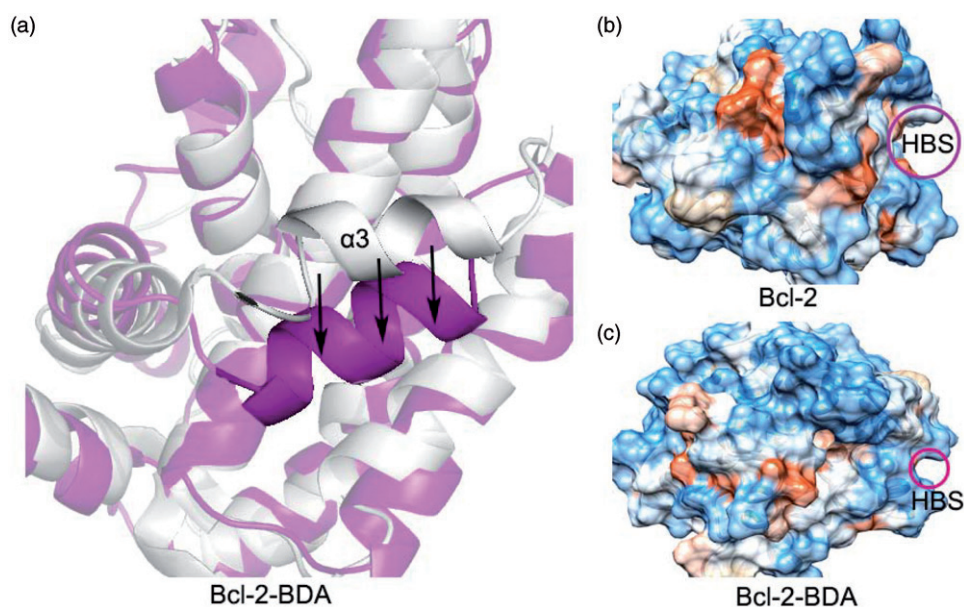


Figure 3. (a) Superimposition of the crystal structure (white) with the representative conformation of simulated Bcl-2-BDA-366 (purple). (b and c) The HBS in representative conformations of simulated Bcl-2 and Bcl-2-BDA-366, respectively.

module of AMBER 16 (Supporting Information File1, File 2). To keep all systems neutral, Na^+ ions were added based on a coulomb potential grid. Systems were then solvated with the TIP3P water model in a truncated octahedron box with a 10 Å distance around the solute (Jorgensen, Chandrasekhar, Madura, Impey, & Klein, 1983), and minimized over 5000 steps of steepest descent minimization, followed by 7000 steps of conjugate gradient minimization. Subsequently, the systems were heated from 0 K to 310 K by Langevin dynamics with collision frequency 1 ps^{-1} , equilibrated over 500 ps, and simulated for 100 ns with time step of 2 fs. Short range interactions were cut off at 12 Å, and bonds involving hydrogen were held fixed using SHAKE.

aMD simulation

The aMD threshold potential and acceleration parameter (α) were calculated according to Donald et al (Hamelberg et al., 2004; Li, Sun, Li, & Lin, 2016), based on 100 ns of conventional MD. Briefly, the potential was modified according to equation:

$$V(r)^* = V(r) + \Delta V(r) \quad (1)$$

$$\Delta V(r) = \frac{(E_p - V(r))^2}{(\alpha P + E_p - V(r))} + \frac{(E_d - V_d(r))^2}{\alpha D + E_d - V_d(r)} \quad (2)$$

where $V(r)$ and $V_d(r)$ are the normal and torsion potential, while E_p and E_d are the average potential and dihedral energies that serve as a reference energy from which to compare the present position of the simulation and, therefore, the relationship to the boosting factor will be applied. αP and αD are factors that determine inversely the strength with which the boost is applied. The Bcl-2-Bid and Bcl-2-Bid-BDA-366 complexes were thus simulated by aMD for 500 ns in AMBER 16, using the ff14SB force field, whereas Bcl-2-BDA-366 complex was simulated for 1 μs . For single ligands BDA-366 and Bid, additional 500 ns aMD simulations were performed for each model under the same conditions as above.

Principal components analysis

Principal components analysis was performed in ProDy (Amadei et al., 1993; Bakan, Meireles, & Bahar, 2011) to resolve the conformational space into essential subspaces that contain several degrees of freedom and describe the motions of the protein. Briefly, the motions of a structure along the trajectory were determined by diagonalization of a covariance matrix of the coordinates of conformations sampled from aMD simulations. To obtain the dominant motion in aMD, the trajectory was then projected along the direction described by a selected eigenvector. Subsequently, the primary motions of the protein were obtained by calculating the two largest projections on the average structure. Simulations were visualized in VMD, and figures were created with PyMOL and chimera (Humphrey, Dalke, & Schulten, 1996; Pettersen et al., 2004; Schrodinger LLC, 2015).

The cluster analysis was performed using the average-linkage hierarchical clustering algorithm obtained from their projection onto the first 2 principal components. The distance from one cluster to another was defined as the average of all distances between individual points of the two clusters. At each iteration step, the two closest clusters were merged. This merging continued until the desired number of clusters was obtained (here was 6 according to the PCA analysis). The representative structures of the clusters were chosen to present the structural information.

Free energy calculations

Binding free energies (ΔG_{bind}) due to the formation of a complex between a ligand and a receptor were calculated by MM-GB/SA with “three-trajectory method” as implemented in AMBER 16 (Rastelli, Del Rio, Degliesposti, &

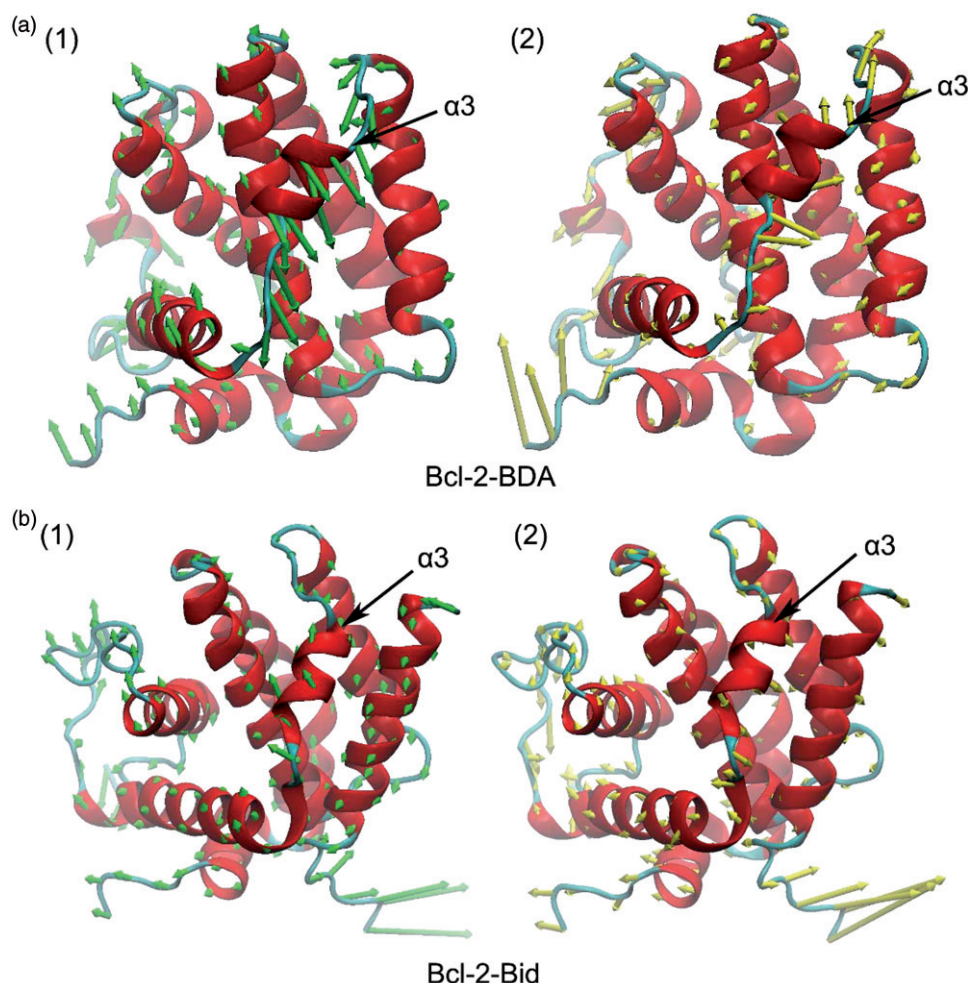


Figure 4. Principal components analysis of Bcl-2-BDA-366 and Bcl-2-Bid, with cones signifying the first (green) and second (yellow) eigenvector movements.

Sgobba, 2010; Sun, Li, Shen, et al., 2014; Sun, Li, Tian, Xu, & Hou, 2014), according to

$$\Delta G_{\text{bind}} = G_{\text{complex}} - (G_{\text{receptor}} + G_{\text{ligand}}) \quad (3)$$

$$E = E_{\text{MM}} + E_{\text{sol}} - T\Delta S \quad (4)$$

$$E_{\text{MM}} = E_{\text{int}} + E_{\text{ele}} + E_{\text{vdw}} \quad (5)$$

$$G_{\text{sol}} = G_{\text{GB}} + G_{\text{SA}} \quad (6)$$

In Equation (4), E_{MM} , E_{sol} , and $T\Delta S$ represent the molecular mechanics component in gas phase, the stabilization energy due to solvation, and a vibrational entropy term, respectively. E_{MM} is calculated in Equation (5) as the sum of E_{intr} , E_{ele} , and E_{vdw} , which are the internal, Coulomb, and van der Waals interaction terms, respectively. Solvation energy, E_{sol} , is deconvoluted into an electrostatic solvation free energy (G_{GB}) and a nonpolar solvation free energy (G_{SA}). The former was obtained by the Generalized Born (GB) method using the GB^{OBC1} model with interior dielectric constant 1, while the latter is considered to be proportional to the molecular solvent accessible surface area (Hou, Zhang, Case, & Wang, 2008). Binding free energies were obtained by averaging values calculated for 500 snapshots extracted from three trajectories of complex at the last 250 ns of simulation.

Results and discussion

BDA-366 induces an allosteric movement of the $\alpha 3$ helix in BH4

Characterization of the conformational changes in Bcl-2 requires overcoming large energy barriers, which are currently inaccessible by conventional MD simulations. To overcome this limitation, we applied an enhanced sampling technique, the aMD. Following initial 100 ns conventional MD simulation, Bcl-2-BDA-366 and Bcl-2-Bid were simulated for 500 ns aMD. BDA-366 was then docked into the representative conformation of the simulated Bcl-2-Bid complex, and the resulting ternary complex was simulated for another 500 ns aMD simulation. The total RMSD from all backbone atoms were generally restricted to a narrow range in Bcl-2-Bid and Bcl-2-Bid-BDA-366, indicating that these structures remained in relatively converged conformations (Figure S1). However, RMSD values increased in Bcl-2-BDA-366 after approximately 350 ns, suggesting nonconvergent simulation. Extension of the simulation to 1 μ s resulted in smaller RMSD oscillations of less than 1 Å (Figure S2), indicating that a stable structure had been reached. Accordingly, all subsequent analyses were based on trajectories of 1000 ns for Bcl-2-BDA-366, 500 ns for Bcl-2-Bid, and 500 ns for Bcl-2-Bid-BDA-366.

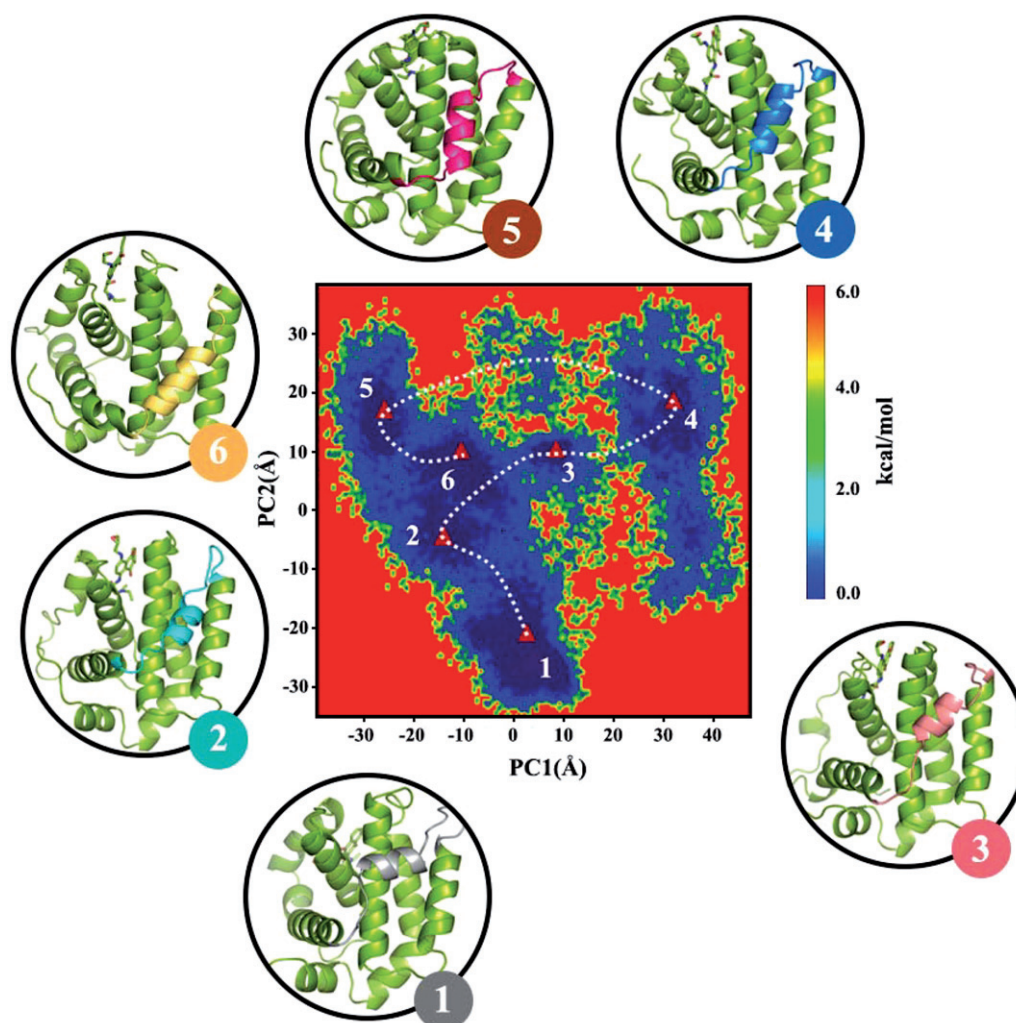


Figure 5. Two-dimensional free energy profiles of the first and second principal components in Bcl-2-BDA-366 complex simulated for 500 ns aMD. The dominant conformational clusters along aMD trajectory are numbered from 1 to 6. Structure 1 presents the open state, structures 2–5 illustrate the semiclosed states, and structure 6 shows the fully closed state.

The representative structures based on the clustering analysis were superimposed with each other to obtain the preliminary estimation of the conformational changes among these complexes. As shown in Figure 3(a), most conformational changes occurred in $\alpha 3$ helix. The $\alpha 3$ underwent translational motion after binding of BDA-366 to the BH4 domain in Bcl-2. As a result, the adjacent HBS in the BH3 domain was severely occluded and inaccessible to its own ligands, including the BH3 peptide.

To characterize dominant conformational states, the aMD trajectory was subjected to principal component analysis (PCA) on Bcl-2-BDA-366 and Bcl-2-Bid. The two largest projections on representative structures were illustrated in Figure 4. In Bcl-2-BDA-366, the first principal component accounted for 39.5% of the total variance, with fairly large conformational variations in $\alpha 3$. The second principal component captures 15.7% of the total variance, which was attributed to a large motion at the C-terminus, and to an exceedingly twisting extension of $\alpha 3$. In contrast, $\alpha 3$ fluctuated more or less *in situ* in the first and second principal components in Bcl-2-Bid.

As observed on the free energy landscape plotted against the two major principal components after reweighting, Bcl-2-

Bid was confined to a well-defined field of energy minima throughout the simulation, while Bcl-2-BDA-366 highlighted an ensemble of different conformational states distributed over a large free energy space (Figure S3). Six representative structures were clearly identified, encompassing the open, closed and semiclosed conformations of the HBS (Figure 5). The most two populated free energy minima corresponded to the open (1.6, -23.2) and fully closed (-7.2, 9.8) states. Projection of Bcl-2-BDA-366 aMD trajectory onto PC sub-space characterized two dominant motions of $\alpha 3$ region throughout the transition: (1) A large-scale helical motion of $\alpha 3$ helix from perpendicular to parallel to $\alpha 4$ helix to form a semiclosed state of the HBS, that was observed when the conformer population shifts from state 1 to state 4 and (2) A downward movement to fully hinder the HBS, that was observed when the system shifts population from state 5 to 6. Combination of these two local motions constituted an “open-semiclosed-closed” transition pathway of the HBS in Bcl-2. Therefore, these results confirmed the recently suggested hypothesis that BDA-366 binds Bcl-2 inducing a conformational change (Han et al., 2015). On the contrary, in Bcl-2-Bid complex the free energy basin was relatively more

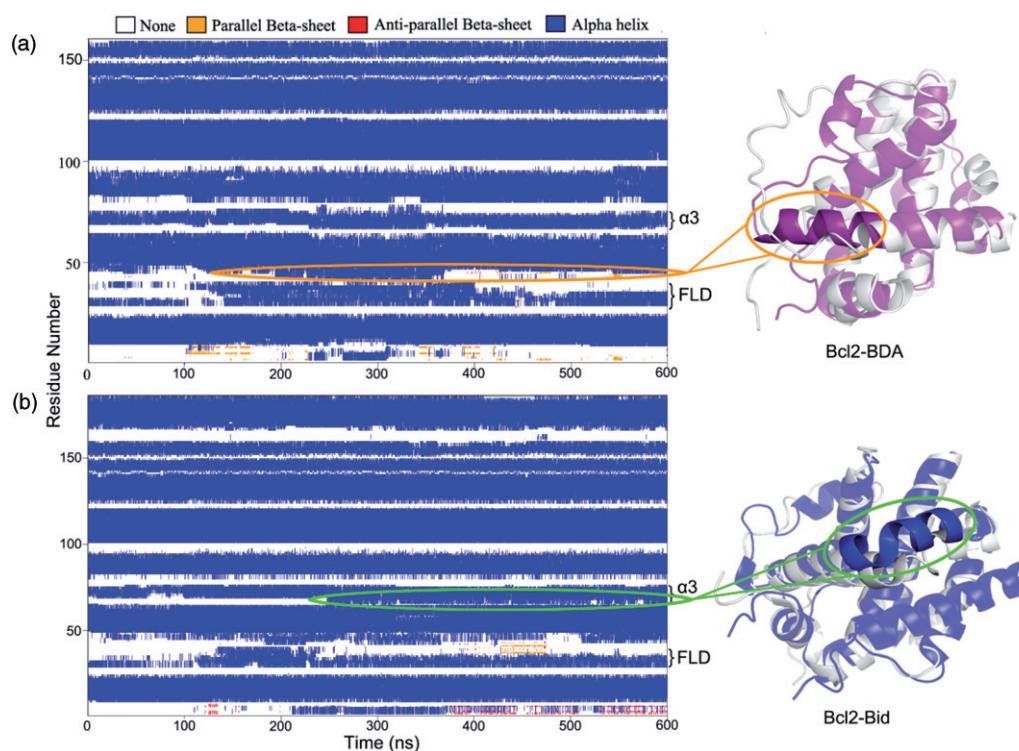


Figure 6. Analysis of the secondary structure in Bcl-2-BDA-366 (a), Bcl-2-Bid (b), and superimposition of the crystal structure (white) with representative conformations of simulated Bcl-2-BDA-366 (a, purple) and Bcl-2-Bid (b, blue).

Table 1. Occupancy of hydrogen bonds among key residues in the BH4 domain.

Hydrogen bond	Occupancy (%)	
	Bcl-2-BDA-366	Bcl-2-Bid
Trp30@O-Asp34@H	None found	87.86
Trp30@O-Ala32@H	51.35	11
Asp31@O-Asp35@H	None found	77.86
Ala32@O-Val36@H	None found	58.23
Val36@O-Arg40@H	89.69	None found

centralized than Bcl-2-BDA-366, as shown in Figure S3, which suggested Bcl-2-Bid mostly fluctuated *in situ*.

The apo form of Bcl-2 was then simulated by aMD for 1 μ s to examine whether the observed conformational changes were due to binding of BDA-366 or to the absence of Bid. During this simulation, the HBS expanded and became more accessible to BH3-only proteins. As shown in Figure 3(b,c), the volume of the HBS, as measured using the online server CASTp (<http://sts.bioe.uic.edu/castp/>) (Binkowski, Naghibzadeh, & Liang, 2003), was 63.2 \AA^3 in Bcl-2-BDA-366, 265.9 \AA^3 in apo Bcl-2 simulated for 1 μ s by aMD, and 265 \AA^3 in crystal structure (PDB: 1G5M), suggesting that α 3 motions were mainly attributable to BDA-366 binding rather than absence of Bid.

Emerging immunoprecipitation and fluorescence polarization assays indicated that novel antagonist-induced conformational changes in Bcl-2 suppress growth of lung cancer xenografts derived from cell lines. Moreover, a mix of Bcl-2 and BDA-366, rather than Bcl-2 alone, was shown to enhance the ability of Bax to bind the 6A7 antibody, whereas BDA-366 itself did not activate Bax (Han et al., 2015). Such behaviors were consistent with the simulations, in which the HBS was occluded as a result of conformational changes in α 3 on binding of BDA-366,

thereby preventing the sequestration of BH3-only proteins. Consequently, BH3-only proteins were free to activate Bax and Bak.

Underlying mechanism of conformational changes induced by BDA-366

The plastic behavior of α 3 helix was further exemplified by the folding of the N-terminus of BH3 (Figure 6(a)), with the α -helical content substantially increasing by 55.1% and 76.5% relative to Bcl-2-Bid and apo Bcl-2, respectively. Binding of Bid also caused the loop between α 2 and α 3 to form a large BH3 helix at approximately 150 ns of aMD, which best agreed with experimental X-ray Bcl-2 structures bound with BH3-mimetic inhibitors (Bruncko et al., 2007; Oltersdorf et al., 2005; Perez et al., 2012) (e.g., PDB: 2O2F, 4AQ3) (Figure 6(b)).

Over the entire simulation, the average occupancy of helix at residues 65-80 (loop α 2-3 + α 3) were 51.12%, 69.8%, and 40.12%, respectively, in Bcl-2-BDA-366, Bcl-2-Bid, and apo Bcl-2. These structural differences indicated that refolding of the α 2- α 3 segment in Bcl-2-Bid may stabilize the region around the HBS and thus promote recruitment of BH3-only proteins, whereas BDA-366 accelerated the folding of the N-terminus of BH3 that led to the concomitant conformational changes. More details can be achieved by hydrogen bonding analysis, and showing how BDA-366 binding affected the folding of BH3 region (Table 1). In Bcl-2-Bid, the backbone atoms of residues Trp30 to Val36 formed a stable hydrogen bond network stabilizing a short helix (Table 1 and Figure 7(a)). On BDA-366 binding, however, Pro127 and Trp30 reoriented their side chains to form significant π - π interactions with the aromatic

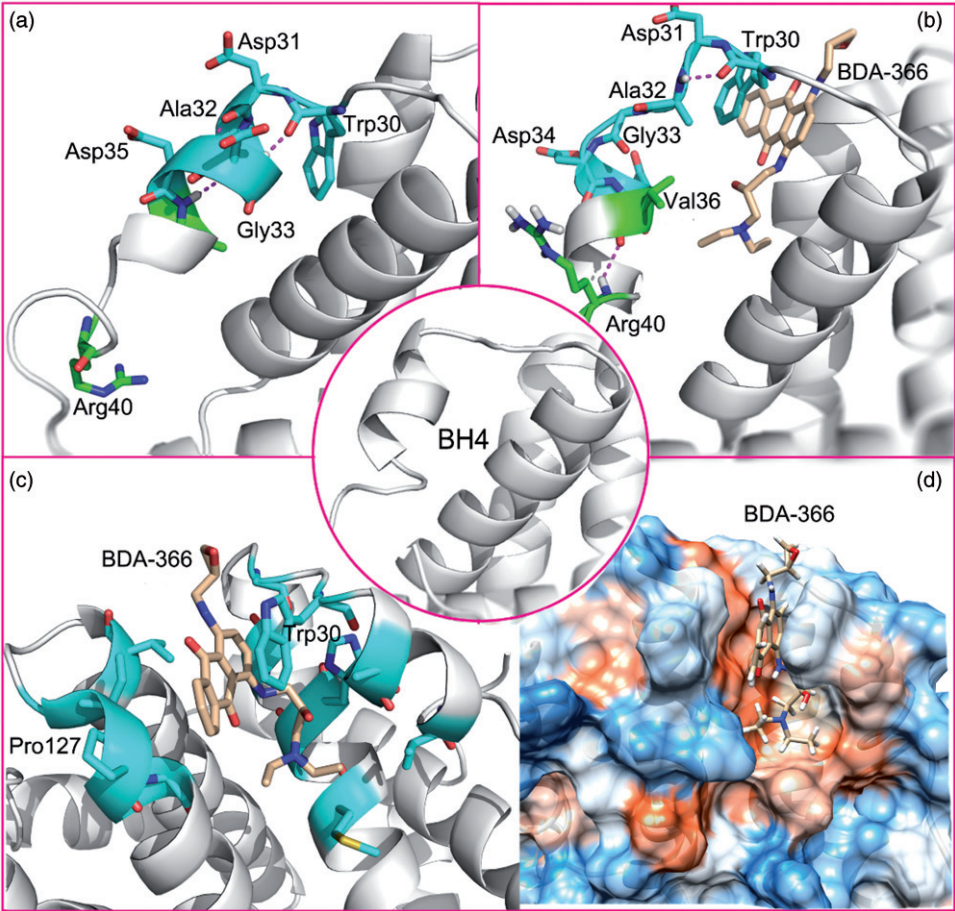


Figure 7. The BH4 domain in representative conformations of simulated Bcl-2-Bid (a) and Bcl-2-BDA-366 (b–d), with the backbone illustrated in the inset. Hydrogen bonds are drawn in magenta dotted line.

Table 2. Binding free energy components for the binary and the ternary complexes using the three-trajectory protocol (kcal·mol^{−1}).

System	Bcl-2-BDA-366	Bcl-2-Bid	Bcl-2-Bid-BDA-366	Bcl-2-BDA-366-Bid
ΔE_{int}	5.05 ± 3.19	125.95 ± 7.23	11.65 ± 3.27	100.55 ± 7.57
ΔE_{vdw}	−28.77 ± 1.71	−143.60 ± 4.49	−7.04 ± 2.14	−58.22 ± 3.84
ΔE_{ele}	−193.87 ± 7.44	−374.94 ± 9.25	−109.03 ± 6.11	−225.86 ± 7.12
ΔG_{GB}	176.29 ± 6.07	287.64 ± 7.04	82.78 ± 5.19	100.69 ± 6.12
ΔG_{SA}	−4.67 ± 0.29	−17.62 ± 0.28	−21.97 ± 0.30	−19.82 ± 0.84
$\Delta G_{\text{MMGB-SA}}^a$	−45.97 ± 4.59	−122.57 ± 6.44	−43.61 ± 3.98	−102.66 ± 5.67
− $T\Delta S$	20.39 ± 3.17	59.65 ± 4.02	26.54 ± 3.24	63.65 ± 4.92
ΔG_{bind}^b	−25.58 ± 4.88	−62.92 ± 6.61	−17.07 ± 4.18	−39.01 ± 6.26

^a $\Delta G_{\text{MMGB-SA}} = \Delta E_{\text{int}} + \Delta E_{\text{vdw}} + \Delta E_{\text{ele}} + \Delta G_{\text{GB}} + \Delta G_{\text{SA}}$

^b $\Delta G_{\text{bind}} = \Delta G_{\text{MMGB-SA}} - T\Delta S$

ring of the ligand (Figure 7(b,c)), in addition to the evident hydrophobic interactions contributed by the strongly hydrophobic binding pocket (Met16, Ile19, Leu23, Tyr28, Val36, Val121, Met125, Leu128, and Val129) (Figure 7(d)).

Consequently, these interactions broke the native hydrogen bonds in the BH4 domain. For example, Ala32, rather than Asp34, donated a new hydrogen bond to the backbone oxygen of Trp30, and the hydrogen bonds within Asp31–Asp35 and Ala32–Val36 were disrupted. Ultimately, these alterations shortened the flexible loop domain and promoted the folding of the BH3 N-terminus into a stable helix. Therefore, the refolded BH3 domain seemed to act as a pry bar that levered $\alpha 3$ downward, while Trp30 in the BH4 domain largely acted as a trigger of the required conformational changes.

Negative cooperative effect of BDA-366 on Bid

To further examine whether BDA-366 impacts the interaction between Bcl-2 and Bid, the Bcl-2-Bid-BDA-366 ternary complex structure was simulated for 500 ns by aMD. Then, binding free energies were analyzed by MM-GB/SA and listed in Table 2. To clearly discern the contributions of the binding free energy of each residue, the energies were decomposed into individual residue contributions (Tables S1–S4). As listed in Table 2 and Tables S1 and S2, Bid binding had little effect on the binding affinity for BDA-366. On the contrary, BDA-366 exhibited relatively large negative cooperative effects on Bid binding, as suggested by a decreased binding free energy by ~ 24 kcal·mol^{−1} with respect to Bcl-2-Bid. Conversely, the binding free energy of Bid was about twice to that of BDA-366, which may explain dose-dependent apoptosis in tumor tissues treated with BDA-366.

Based on the analysis of energy terms, the reduction in binding free energy of Bid in Bcl2-Bid-BDA-366 complex compared to that in Bcl2-Bid complex were attributed to both the electrostatic and the van-der-Waals interactions. Remarkably, the electrostatic contributions for Bid binding were decreased in the ternary complex than in the binary complex by -149.08 kcal·mol^{−1}, which may be due to the disruption of the hydrogen bond network between Bid and the residues in HBS. In particular, residues Glu94, Glu95, Asp99,

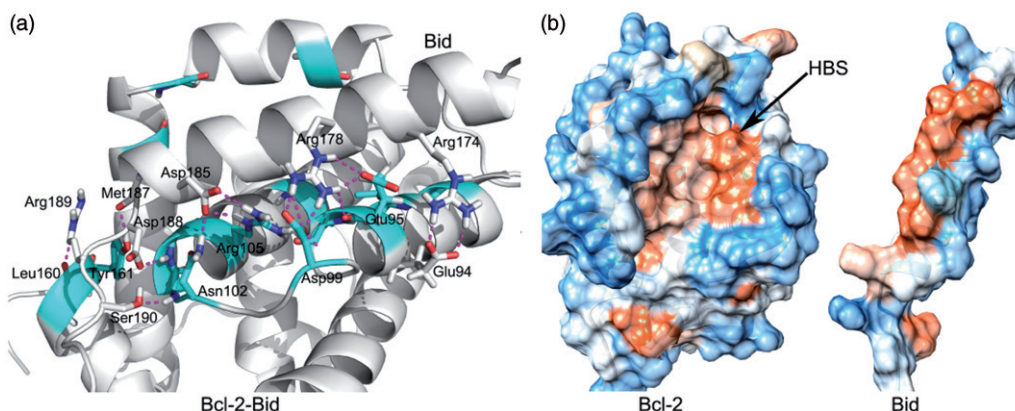


Figure 8. (a) Decomposition of binding free energy on a per-residue basis in Bcl-2-Bid (cyan), and hydrogen bonds formed between Bid and Bcl-2 (magenta dashed line). (b) Hydrophobic surface in the HBS in Bcl-2-Bid.

Table 3. Occupancy of hydrogen bonds between key residues in Bcl-2-Bid and Bcl-2-Bid-BDA-366.

Hydrogen bond	Occupancy (%)	
	Bcl-2-Bid	Bcl-2-Bid-BDA-366
Glu94@O-Arg174@H	21.34	6.39
Glu95@O-Arg178@H	43.58	21.98
Asp99@O-Arg178@H	30.78	27.27
Asp185@O-Asn102@H	43.60	36.63
Ser190@O-Trp103@H	51.27	None found
Asp188@O-Gly104@H	42.33	36.26
Asp185@O-Arg105@H	87.70	86.41
Leu160@O-Arg189@H	14.23	6.59
Met187@O-Tyr161@H	65.62	32.87

Asn102, Trp103, Gly104, Arg105, Leu160, and Tyr161 in Bcl-2-Bid complex formed a hydrogen bond network that stabilize Bid as shown in Figure 8(a), in addition to strong hydrophobic interactions (Figure 8(b)). When BDA-366 was bound to the BH4 domain of Bcl2-Bid complex, the occupancies of the hydrogen bonds were severely reduced or even disappeared (Table 3).

In addition, consistent results can also be found in analyzing the decomposition of binding free energy on per-residue (Tables S3–S4), as the binding free energy of residues Glu94, Glu95, Asp99, Asn102, Trp103, Arg105, Leu160 were decreased obviously under BDA-366 binding to the BH4 domain. Intriguingly, the binding free energies of two exceptions residues Gly104, and Tyr161 were increased contrarily in Bcl2-Bid-BDA-366 complex, which maybe resulted from the distortion of the C-terminal of Bid induced by the disruption of the hydrogen bond network. Thereby, BDA-366 was suggested to disrupt the hydrogen bond network as listed in Table 3, resulting the reduction of the binding affinity for Bid.

Conclusion

Despite the cognizance of targeting the BH3 domain to generate Bcl-2 inhibitors for cancer therapy over the past decades, targeting the specific BH4 domain of Bcl-2 has become a novel strategy for cancer therapy. Bcl-2 via the BH4 domain could interact with multiple proteins, such as apoptosis-stimulating p53 protein 2 (ASPP2), inositol 1,4,5-trisphosphate receptor, and voltage-dependent anion channel, that participate in numerous signaling pathways (Deng, Gao, & May,

2009). Recently, small molecule BDA-366 has been observed as a potent and effective BH4 domain antagonist that converts the Bcl-2 antiapoptotic function. Despite such tremendous advances, X-ray structures represent only static snapshots of Bcl-2 apo structure without BDA-366 bound during cell apoptotic processes. Detail mechanisms of this important functional conversion remain unclear. In this study, we applied aMD to gain insight into the underlying mechanism for the functional conversion of Bcl-2 from a survival molecule to a cell death inducer in apoptosis regulation caused by BDA-366. By docking inside the BH4 domain and subsequently 1 μ s aMD simulations, BDA-366 was observed to induce the downward movement of α 3 region and then block HBS or contribute negative cooperativity effect to reduce Bid binding affinity. Therefore, the BH4 domain antagonist BDA-366 was suggested to act as a “sensitizer” that released BH3-only activator proteins by blocking the HBS or reducing the binding affinity to further avidly promote mitochondrial outer membrane permeabilization through activation and oligomerization of Bax and Bak. Overall, the aMD simulations presented in this study provides structural clues of how conformational changes may get induced by BDA-366 in α 3 region of Bcl-2, which are relevant to the unresolved issues of Bcl-2 functional conversion. A negative cooperative model was identified to reveal the inhibiting effect between the BH3 and BH4 domains. Furthermore, this study may also provide some inspirations for the molecular mechanism of Bcl-2 in apoptosis regulation.

Disclosure statement

There are no interest conflicts to declare.

Funding

This work is supported by the National Natural Science Foundation of China [21603013, 31601412]; 100 Talent Program grant and Biological Resources Service Network Initiative [ZSYS-012]; Chinese Academy of Sciences [SKT1604].

ORCID

Bian Wu <http://orcid.org/0000-0002-6524-2049>

References

- Acoca, S., Cui, Q., Shore, G. C., & Purisima, E. O. (2011). Molecular dynamics study of small molecule inhibitors of the Bcl-2 family. *Proteins*, 79(9), 2624–2636. doi:10.1002/prot.23083
- Amadei, A., Linssen, A. B. M., & Berendsen, H. J. C. (1993). Essential dynamics of proteins. *Proteins: Structure, Function, and Bioinformatics*, 17(4), 412–425. doi:10.1002/prot.340170408
- Andersen, O. J., Risor, M. W., Poulsen, E. C., Nielsen, N. C., Miao, Y., Enghild, J. J., & Schiott, B. (2017). Reactive center loop insertion in alpha-1-antitrypsin captured by accelerated molecular dynamics simulation. *Biochemistry*, 56(4), 634–646. doi:10.1021/acs.biochem.6b00839
- Antignani, A., & Youle, R. J. (2006). How do Bax and Bak lead to permeabilization of the outer mitochondrial membrane? *Current Opinion in Cell Biology*, 18(6), 685–689. doi:10.1016/j.ceb.2006.10.004
- Bakan, A., Meireles, L. M., & Bahar, I. (2011). ProDy: Protein dynamics inferred from theory and experiments. *Bioinformatics*, 27(11), 1575–1577. doi:10.1093/bioinformatics/btr168
- Binkowski, T. A., Naghibzadeh, S., & Liang, J. (2003). CASTp: Computed Atlas of Surface Topography of proteins. *Nucleic Acids Research*, 31(13), 3352–3355.
- Bruncko, M., Oost, T. K., Belli, B. A., Ding, H., Joseph, M. K., Kunzer, A., ... Elmore, S. W. (2007). Studies leading to potent, dual inhibitors of Bcl-2 and Bcl-xL. *Journal of Medicinal Chemistry*, 50(4), 641–662. doi:10.1021/jm061152t
- Case, D. A., Betz, R. M., Cerutti, D. S., Cheatham, T., Darden, T., Duke, R. E., & Kollman, P. A. (2016). *AMBER 2016*. San Francisco, CA: University of California.
- Czabotar, P. E., Westphal, D., Dewson, G., Ma, S., Hockings, C., Fairlie, W. D., ... Colman, P. M. (2013). Bax crystal structures reveal how BH3 domains activate Bax and nucleate its oligomerization to induce apoptosis. *Cell*, 152(3), 519–531. doi:10.1016/j.cell.2012.12.031
- Delbridge, A. R., Grabow, S., Strasser, A., & Vaux, D. L. (2016). Thirty years of BCL-2: Translating cell death discoveries into novel cancer therapies. *Nature Reviews Cancer*, 16(2), 99–109. doi:10.1038/nrc.2015.17
- Deng, X., Gao, F., & May, W. S. (2009). Protein phosphatase 2A inactivates Bcl2's antiapoptotic function by dephosphorylation and up-regulation of Bcl2-p53 binding. *Blood*, 113(2), 422–428. doi:10.1182/blood-2008-06-165134
- Do, H., & Troisi, A. (2015). Developing accurate molecular mechanics force fields for conjugated molecular systems. *Physical Chemistry Chemical Physics*, 17(38), 25123–25132. doi:10.1039/c5cp04328j
- Elmore, S. (2007). Apoptosis: a review of programmed cell death. *Toxicologic Pathology*, 35(4), 495–516. doi:10.1080/01926230701320337
- Frisch, M. J., Trucks, G. W., Schlegel, H. B., Scuseria, G. E., Robb, M. A., Cheeseman, J. R., ... Fox, D. J. (2016). *Gaussian 16 Rev. B.01*. Wallingford, CT: Gaussian 09 Rev. A.02.
- Gibson, C. J., & Davids, M. S. (2015). BCL-2 antagonism to target the intrinsic mitochondrial pathway of apoptosis. *Clinical Cancer Research*, 21(22), 5021–5029. doi:10.1158/1078-0432.ccr-15-0364
- Hamelberg, D., Mongan, J., & McCammon, J. A. (2004). Accelerated molecular dynamics: A promising and efficient simulation method for biomolecules. *The Journal of Chemical Physics*, 120(24), 11919–11929. doi:10.1063/1.1755656
- Han, B., Park, D., Li, R., Xie, M., Owonikoko, T. K., Zhang, G., ... Deng, X. (2015). Small-molecule Bcl2 BH4 antagonist for lung cancer therapy. *Cancer Cell*, 27(6), 852–863. doi:10.1016/j.ccell.2015.04.010
- Hardwick, J. M., & Soane, L. (2013). Multiple functions of BCL-2 family proteins. *Cold Spring Harbor Perspectives Biology*, 5(2), 152–158. doi:10.1101/cshperspect.a008722
- Hou, T., Zhang, W., Case, D. A., & Wang, W. (2008). Characterization of domain-peptide interaction interface: A case study on the amphipysin-1 SH3 domain. *Journal of Molecular Biology*, 376(4), 1201–1214. doi:10.1016/j.jmb.2007.12.054
- Humphrey, W., Dalke, A., & Schulten, K. (1996). VMD: Visual molecular dynamics. *Journal of Molecular Graphics*, 14(1), 33–38, 27–38.
- Jorgensen, W. L., Chandrasekhar, J., Madura, J. D., Impey, R. W., & Klein, M. L. (1983). Comparison of simple potential functions for simulating liquid water. *The Journal of Chemical Physics*, 79(2), 926–935. doi:10.1063/1.445869
- Kalenkiewicz, A., Grant, B. J., & Yang, C. Y. (2015). Enrichment of drug-gable conformations from apo protein structures using cosolvent-accelerated molecular dynamics. *Biology (Basel)*, 4(2), 344–366. doi:10.3390/biology4020344
- Kerr, J. F., Wyllie, A. H., & Currie, A. R. (1972). Apoptosis: A basic biological phenomenon with wide-ranging implications in tissue kinetics. *British Journal of Cancer*, 26(4), 239–257.
- Kolluri, S. K., Zhu, X., Zhou, X., Lin, B., Chen, Y., Sun, K., ... Zhang, X. K. (2008). A short Nur77-derived peptide converts Bcl-2 from a protector to a killer. *Cancer Cell*, 14(4), 285–298. doi:10.1016/j.ccr.2008.09.002
- Koshy, C., Parthiban, M., & Sowdhamini, R. (2010). 100 ns molecular dynamics simulations to study intramolecular conformational changes in Bax. *Journal of Biomolecular Structure and Dynamics*, 28(1), 71–83. doi:10.1080/07391102.2010.10507344
- Ku, B., Liang, C., Jung, J. U., & Oh, B. H. (2011). Evidence that inhibition of BAX activation by BCL-2 involves its tight and preferential interaction with the BH3 domain of BAX. *Cell Research*, 21(4), 627–641. doi:10.1038/cr.2010.149
- Li, Y., Sun, J., Li, D., & Lin, J. (2016). Activation and conformational dynamics of a class B G-protein-coupled glucagon receptor. *Physical Chemistry Chemical Physics*, 18(18), 12642–12650. doi:10.1039/c6cp00798h
- Liu, Z., Wild, C., Ding, Y., Ye, N., Chen, H., Wold, E. A., & Zhou, J. (2016). BH4 domain of Bcl-2 as a novel target for cancer therapy. *Drug Discovery Today*, 21(6), 989–996. doi:10.1016/j.drudis.2015.11.008
- Lopez, J., & Tait, S. W. (2015). Mitochondrial apoptosis: Killing cancer using the enemy within. *British Journal of Cancer*, 112(6), 957–962. doi:10.1038/bjc.2015.85
- Markwick, P. R., & McCammon, J. A. (2011). Studying functional dynamics in bio-molecules using accelerated molecular dynamics. *Physical Chemistry Chemical Physics*, 13(45), 20053–20065. doi:10.1039/c1cp22100k
- Miao, Y., Feixas, F., Eun, C., & McCammon, J. A. (2015). Accelerated molecular dynamics simulations of protein folding. *Journal of Computational Chemistry*, 36(20), 1536–1549. doi:10.1002/jcc.23964
- Miles, J. A., Yeo, D. J., Rowell, P., Rodriguez-Marin, S., Pask, C. M., Warriner, S. L., ... Wilson, A. J. (2016). Hydrocarbon constrained peptides – Understanding preorganisation and binding affinity. *Chemical Science*, 7(6), 3694–3702. doi:10.1039/C5SC04048E
- Moldoveanu, T., Follis, A. V., Kriwacki, R. W., & Green, D. R. (2014). Many players in BCL-2 family affairs. *Trends in Biochemistry Sciences*, 39(3), 101–111. doi:10.1016/j.tibs.2013.12.006
- Moldoveanu, T., Grace, C. R., Llambi, F., Nourse, A., Fitzgerald, P., Gehring, K., ... Green, D. R. (2013). BID-induced structural changes in BAK promote apoptosis. *Nature Structural and Molecular Biology*, 20(5), 589–597. doi:10.1038/nsmb.2563
- Morris, G. M., Huey, R., Lindstrom, W., Sanner, M. F., Belew, R. K., Goodsell, D. S., & Olson, A. J. (2009). AutoDock4 and AutoDockTools4: Automated docking with selective receptor flexibility. *Journal of Computational Chemistry*, 30(16), 2785–2791. doi:10.1002/jcc.21256
- Ola, M. S., Nawaz, M., & Ahsan, H. (2011). Role of Bcl-2 family proteins and caspases in the regulation of apoptosis. *Molecular and Cellular Biochemistry*, 357(1–2), 41–58. doi:10.1007/s11010-010-0709-x
- Oltersdorf, T., Elmore, S. W., Shoemaker, A. R., Armstrong, R. C., Augeri, D. J., Belli, B. A., ... Rosenberg, S. H. (2005). An inhibitor of Bcl-2 family proteins induces regression of solid tumours. *Nature*, 435(7042), 677–681. doi:10.1038/nature03579
- Perez, H. L., Banfi, P., Bertrand, J., Cai, Z. W., Grebinski, J. W., Kim, K., ... Borzilleri, R. M. (2012). Identification of a phenylacetylsulfonamide series of dual Bcl-2/Bcl-xL antagonists. *Bioorganic and Medicinal Chemistry Letters*, 22(12), 3946–3950. doi:10.1016/j.bmcl.2012.04.103
- Petros, A. M., Medek, A., Nettesheim, D. G., Kim, D. H., Yoon, H. S., Swift, K., ... Fesik, S. W. (2001). Solution structure of the antiapoptotic protein bcl-2. *Proceedings of the National Academy of Sciences of the United States of America*, 98(6), 3012–3017. doi:10.1073/pnas.041619798
- Pettersen, E. F., Goddard, T. D., Huang, C. C., Couch, G. S., Greenblatt, D. M., Meng, E. C., & Ferrin, T. E. (2004). UCSF Chimera—A visualization

- system for exploratory research and analysis. *Journal of Computational Chemistry*, 25(13), 1605–1612. doi:[10.1002/jcc.20084](https://doi.org/10.1002/jcc.20084)
- Pierce, B. G., Wiehe, K., Hwang, H., Kim, B. H., Vreven, T., & Weng, Z. (2014). ZDOCK server: Interactive docking prediction of protein-protein complexes and symmetric multimers. *Bioinformatics*, 30(12), 1771–1773. doi:[10.1093/bioinformatics/btu097](https://doi.org/10.1093/bioinformatics/btu097)
- Raghav, P. K., Verma, Y. K., & Gangenahalli, G. U. (2012). Molecular dynamics simulations of the Bcl-2 protein to predict the structure of its unordered flexible loop domain. *Journal of Molecular Modeling*, 18(5), 1885–1906. doi:[10.1007/s00894-011-1201-6](https://doi.org/10.1007/s00894-011-1201-6)
- Rajan, S., Choi, M., Baek, K., & Yoon, H. S. (2015). Bh3 induced conformational changes in Bcl-Xl revealed by crystal structure and comparative analysis. *Proteins*, 83(7), 1262–1272. doi:[10.1002/prot.24816](https://doi.org/10.1002/prot.24816)
- Rastelli, G., Del Rio, A., Degliesposti, G., & Sgobba, M. (2010). Fast and accurate predictions of binding free energies using MM-PBSA and MM-GBSA. *Journal of Computational Chemistry*, 31(4), 797–810. doi:[10.1002/jcc.21372](https://doi.org/10.1002/jcc.21372)
- Schrodinger, LLC. (2015). *The PyMOL Molecular Graphics System, Version 1.8*. New York, NY: Author.
- Shamas-Din, A., Kale, J., Leber, B., & Andrews, D. W. (2013). Mechanisms of action of Bcl-2 family proteins. *Cold Spring Harbor Perspectives Biology*, 5(4), a008714. doi:[10.1101/cshperspect.a008714](https://doi.org/10.1101/cshperspect.a008714)
- Shao, J., Tanner, S. W., Thompson, N., & Cheatham, T. E. (2007). Clustering molecular dynamics trajectories: 1. Characterizing the performance of different clustering algorithms. *Journal of Chemical Theory and Computation*, 3(6), 2312–2334. doi:[10.1021/ct700119m](https://doi.org/10.1021/ct700119m)
- Sun, H., Li, Y., Shen, M., Tian, S., Xu, L., Pan, P., ... Hou, T. (2014). Assessing the performance of MM/PBSA and MM/GBSA methods. 5. Improved docking performance using high solute dielectric constant MM/GBSA and MM/PBSA rescoring. *Physical Chemistry Chemical Physics*, 16(40), 22035–22045. doi:[10.1039/c4cp03179b](https://doi.org/10.1039/c4cp03179b)
- Sun, H., Li, Y., Tian, S., Xu, L., & Hou, T. (2014). Assessing the performance of MM/PBSA and MM/GBSA methods. 4. Accuracies of MM/PBSA and MM/GBSA methodologies evaluated by various simulation protocols using PDBbind data set. *Physical Chemistry Chemical Physics*, 16(31), 16719–16729. doi:[10.1039/c4cp01388c](https://doi.org/10.1039/c4cp01388c)
- Thomas, S., Quinn, B. A., Das, S. K., Dash, R., Emdad, L., Dasgupta, S., ... Fisher, P. B. (2013). Targeting the Bcl-2 family for cancer therapy. *Expert Opinion on Therapeutic Targets*, 17(1), 61–75. doi:[10.1517/14728222.2013.733001](https://doi.org/10.1517/14728222.2013.733001)
- Toure, B. B., Miller-Moslin, K., Yusuff, N., Perez, L., Dore, M., Joud, C., ... Visser, M. (2013). The role of the acidity of N-heteroaryl sulfonamides as inhibitors of bcl-2 family protein-protein interactions. *ACS Medicinal Chemistry Letters*, 4(2), 186–190. doi:[10.1021/ml300321d](https://doi.org/10.1021/ml300321d)
- Vela, L., & Marzo, I. (2015). Bcl-2 family of proteins as drug targets for cancer chemotherapy: The long way of BH3 mimetics from bench to bedside. *Current Opinion in Pharmacology*, 23, 74–81. doi:[10.1016/j.coph.2015.05.014](https://doi.org/10.1016/j.coph.2015.05.014)
- Willis, S. N., Fletcher, J. I., Kaufmann, T., van Delft, M. F., Chen, L., Czabotar, P. E., ... Huang, D. C. (2007). Apoptosis initiated when BH3 ligands engage multiple Bcl-2 homologs, not Bax or Bak. *Science*, 315(5813), 856–859. doi:[10.1126/science.1133289](https://doi.org/10.1126/science.1133289)